

## Article

# Interaction Regularity of Biomolecules on Mg and Mg-Based Alloy Surfaces: A First-Principles Study

Zhe Fang <sup>1,2</sup>, Baiwei Ma <sup>1,\*</sup>, Erjun Liang <sup>2,\*</sup>, Yu Jia <sup>2,3</sup> and Shaokang Guan <sup>4</sup>

<sup>1</sup> School of Materials and Chemical Engineering, Center for Advanced Materials Research, Zhongyuan University of Technology, Zhengzhou 450007, China; zhefang@zut.edu.cn

<sup>2</sup> School of Physics and Microelectronics & International Laboratory for Quantum Functional Materials of Henan, Zhengzhou University, Zhengzhou 450001, China; jiayu@zzu.edu.cn

<sup>3</sup> Key Laboratory for Special Functional Materials of Ministry of Education, Henan University, Kaifeng 475004, China

<sup>4</sup> School of Materials Science and Engineering, Zhengzhou University, Zhengzhou 450001, China; skguan@zzu.edu.cn

\* Correspondence: 6799@zut.edu.cn (B.M.); ejliang@zzu.edu.cn (E.L.)

**Abstract:** Adsorbed molecules can modulate the behavior of magnesium (Mg) and Mg alloy in biomedical applications. The interaction regularity and mechanism of biomolecules (such as amino acids, dipeptides, and tripeptide) on a Mg(0001) surface, the influence of dipole correction, and the effects of alloying elements and electronic structure were investigated in this study using first-principles calculations. Specifically, the adsorption energy ( $E_{ads}$ ) of functional groups (-NH<sub>2</sub>, -COOH and -CN<sub>3</sub>H<sub>4</sub>), amino acids (arginine (Arg), glycine (Gly), and aspartic acid (Asp)), dipeptides (arginine-glycine (Arg-Gly), glycine-aspartic acid (Gly-Asp), and arginine-aspartic acid (Arg-Asp)), and arginine-glycine-aspartic acid (RGD) tripeptide were systematically calculated. Dipole correction slightly enhanced the interaction between molecules and Mg surfaces, but the  $E_{ads}$  trend remained unchanged. The addition of alloying elements improved the interaction of molecules and Mg-based alloy surfaces. This study will be of fundamental importance in understanding the interaction regularity of molecules on Mg and Mg-based alloy surfaces and provide possibilities for surface modification design of biomedical materials.



**Citation:** Fang, Z.; Ma, B.; Liang, E.; Jia, Y.; Guan, S. Interaction Regularity of Biomolecules on Mg and Mg-Based Alloy Surfaces: A First-Principles Study. *Coatings* **2024**, *14*, 25. <https://doi.org/10.3390/coatings14010025>

Academic Editors: Alexander S. Lenshin and Vladimir Kashkarov

Received: 28 November 2023

Revised: 18 December 2023

Accepted: 23 December 2023

Published: 25 December 2023



**Copyright:** © 2023 by the authors. Licensee MDPI, Basel, Switzerland. This article is an open access article distributed under the terms and conditions of the Creative Commons Attribution (CC BY) license (<https://creativecommons.org/licenses/by/4.0/>).

**Keywords:** biomolecules; Mg; interaction regularity; first-principles calculation; dipole correction

## 1. Introduction

The biomolecular coating modified on the surface of biomedical materials is a direct contact site for cell adhesion and growth on the material surface, which has a significant impact on human physiological activities [1–6]. Numerous in vivo and in vitro animal experiments have shown that Mg alloy materials modified with functional biomolecular coatings have good biocompatibility, biomechanical compatibility, antibacterial properties, and appropriate corrosion resistance performance [7–10]. A key point in designing Mg alloy materials with functional surfaces is the formation of biological coatings that improve the adhesion and survival of specific cell types. It is well known that biomolecules such as amino acids, dipeptides, and tripeptides play important roles in the physiological activities of the human body [11–15]. In particular, recent research reports have focused on the preparation of functionally controllable bioactive peptide coatings to enhance anti-infection activity, accelerate vascular endothelialization, and promote vascular tissue healing [16–18]. The bonding properties and interaction regularities between biomolecules and Mg alloy surfaces play a crucial role in the stable existence of functional biomolecular coatings on the alloy surface. Therefore, study of the interaction mechanism between biomolecules and the surface of biomedical Mg alloys will provide a theoretical basis for the selection of functional biomolecular coatings.

Biomolecules (such as amino acids, dipeptides, and tripeptide) provide novel and superior performance for biomedical coatings, and biomolecular coatings bind to the surface of materials through their specific amino acid sequences and active functional groups [19]. Amino and carboxyl groups are important active functional groups in vivo, which often serve as fixed sites for biological macromolecules such as proteins and enzymes in the body due to their high affinity with cells and structural tissues [20,21]. Amino acids are the fundamental components of proteins, and short peptides are simple organic tissue structures formed by amino acids, without the additional complexity of folding [22,23]. Structures of short peptides can serve as units for the chemical synthesis of biological functional molecules, and their complexity can also provide valuable information for regulating the mechanisms of organic–inorganic mixed interfaces. Surface modification of Mg alloys through functional biomolecules has become an important research direction in the functionalization of biomaterials.

Recent theoretical and experimental studies on the interaction mechanism between biomolecules and metal surfaces have proposed some new perspectives [24–26]. Farwa et al. reported a biodegradable Mg alloy stent with a dual effect of drug (Paclitaxel) and growth factor (VEGF) release [27]. Zhang et al. reported the adsorption mechanism and conformation change of bovine serum albumin on the AZ31 Mg substrate and its MAO coatings, using experimental methods and MD simulations [4]. Yuan et al. demonstrated that CaP coatings prepared at 60 °C have higher corrosion resistance compared with coatings prepared at other temperatures through comparative experimental and molecular dynamics simulation studies [28]. Wang et al. found that binary Mg intermetallics could greatly suppress the corrosion cathodic reaction, using active learning and density functional theory (DFT) simulations [29]. Mamad et al. reported that L-glutamine may have the highest inhibitory effect on anti-corrosion performance, confirming their findings through DFT calculations and Monte Carlo simulation [30]. Méthivier et al. studied the adsorption behavior of Glu–Cys–Gly peptide on copper surfaces through electrospray ion beam deposition and DFT calculations and identified the most stable configurations of the peptide in the adsorbed state [31]. Therefore, the interaction regularities of functional molecules on Mg and Mg-based alloy surfaces were investigated to provide a better theoretical basis for the functional biomolecular coatings design.

The interaction mechanism between molecules and different Mg surfaces was investigated in our previous work [32–35]. Nevertheless, the interaction regularity within molecules on magnesium (Mg) and Mg-based alloy surfaces has not been fully understood. In the present work, first-principles calculations based on DFT were employed to study the interaction regularity of functional groups, amino acids, dipeptides, and RGD tripeptide on Mg and Mg-based alloy surfaces. Investigating the interaction regularity of the molecules on Mg and Mg-based alloy surfaces provides a comprehensive understanding for the design of functional biomolecular coatings.

## 2. Computational Methods

All calculations were performed using the Vienna Ab initio Simulation package (VASP) based on the periodic density functional theory (DFT) method [36,37]. The projector-augmented wave (PAW) potentials were used for characterizing the ion and valence electron interactions [38,39], employing the Perdew, Burke and Ernzerhof (PBE) method to deal with the exchange correlation [40]. Dispersion forces were considered in the optB86b-vdW approach [41], and  $3s^23p^0$ ,  $1s^1$ ,  $2s^22p^2$ ,  $2s^22p^3$ , and  $2s^22p^4$  were chosen as the valence electrons for Mg, H, C, N, and O atoms, respectively. The energy cutoff (Ecut) in use was set to 450 eV and a  $1 \times 1 \times 1$  k-point was considered for the Brillouin-zone sampling in this work. An  $8 \times 8$  supercell with a six-layer Mg slab was selected as the surface adsorption model. To minimize the interactions in the z direction between periodic images of the system, the vacuum region was set at more than 20 Å. The bottom two layers of Mg atoms were fixed throughout the optimization and the vacuum region was set at 20 Å to minimize the interactions in the z direction of the periodic adsorption system. Molecules were adsorbed

on the top side of the adsorption surfaces. The optimizations of adsorption systems were considered converged when the ground state reached  $10^{-5}$  eV and the Hellmann–Feynman forces were inferior to  $0.02$  eV/Å.

The binding ability of molecules on the different substrates was characterized by the  $E_{ads}$  which were calculated as follows [42].

$$E_{ads} = E_{mol+sub} - E_{mol} - E_{sub} \quad (1)$$

where  $E_{mol+sub}$ ,  $E_{mol}$ , and  $E_{sub}$  and represent the total energy of the optimized stable adsorption systems, the total energy of the optimized molecules, and the energy of the different substrates, respectively.

### 3. Results and Discussion

To investigate the interaction regularity of molecules on Mg and Mg-based alloy surfaces is important in the biomedical field. In order to make the calculation results much clearer, we labeled the hydrogenated functional groups as  $\text{NH}_3$ ,  $\text{HCOOH}$ , and  $\text{HCN}_3\text{H}_4$ , respectively. For the present work, the optimized structures of  $\text{NH}_3$ ,  $\text{HCOOH}$ ,  $\text{HCN}_3\text{H}_4$ , Arg( $\text{C}_6\text{H}_{14}\text{N}_4\text{O}_2$ ), Gly( $\text{C}_2\text{H}_5\text{NO}_2$ ), Asp( $\text{C}_4\text{H}_7\text{NO}_4$ ), Arg-Gly( $\text{C}_8\text{H}_{17}\text{N}_5\text{O}_3$ ), Gly-Asp( $\text{C}_6\text{H}_{10}\text{N}_2\text{O}_5$ ), Arg-Asp( $\text{C}_{10}\text{H}_{19}\text{N}_5\text{O}_5$ ), and RGD( $\text{C}_{12}\text{H}_{22}\text{N}_6\text{O}_6$ ) tripeptide are depicted in Figure 1a–j. The optimized lattice parameters of the bulk hcp Mg were  $a = b = 3.188$  Å and  $c = 5.193$  Å, which were in good agreement with the experimental results ( $a = b = 3.210$  Å,  $c = 5.213$  Å) [43]. The interaction regularity of functional groups, amino acids, dipeptides, and RGD tripeptide on Mg and Mg-based alloy surfaces were studied as follows.

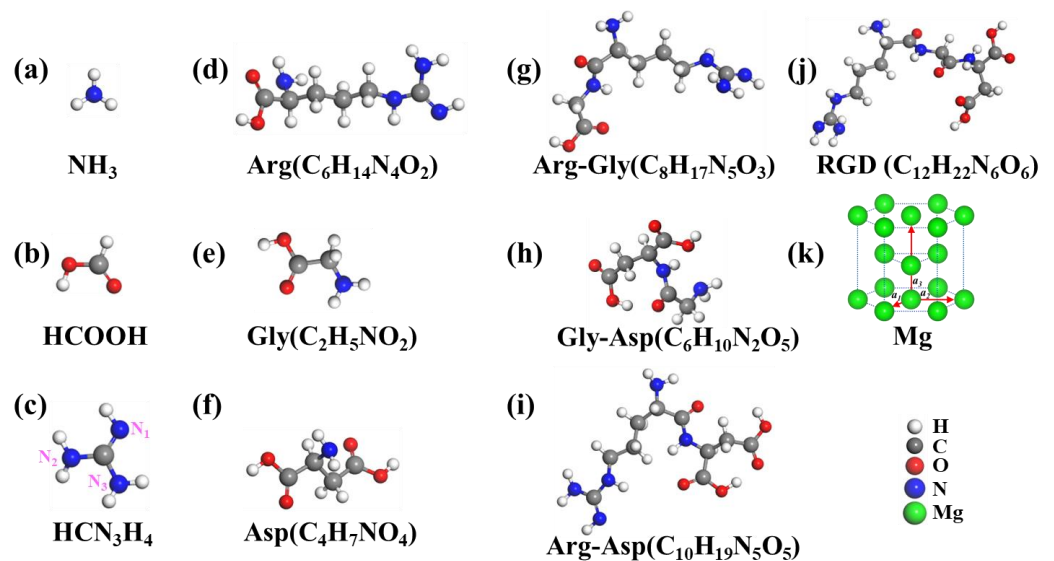


**Figure 1.** Optimized structure of (a–c) functional groups, (d–f) amino acids, (g–i) dipeptides, and (j) RGD tripeptide. The crystal structure of (k) Mg.

#### 3.1. Adsorption Properties of Molecules on Mg(0001) Surfaces

Functional groups play a crucial role in the binding process between functional molecules and metal surfaces. The binding process between the surfaces of biomedical materials and molecules depends on the properties of amino acids and peptides. Madden et al. [44] studied the adsorption behavior of Gly on a Cu(311) surface using a combination of theoretical calculations and experimental methods. The calculated results showed that the adsorption structure of Gly was the most stable when a N atom in the amino group and an O atom in the carboxyl group were simultaneously adsorbed on the Cu(311) surface. The riveting atoms (such as N in the amino/guanidine group or O in the carboxyl group) interact with the surface atoms when biomolecules interact with biomedical surfaces [45]. The adsorption process results in the redistribution of electrons in

the system and the formation of chemical bonds. The stable adsorption configurations of functional groups, amino acids, dipeptides, and RGD tripeptide on Mg(0001) surfaces are represented in Figure 2.

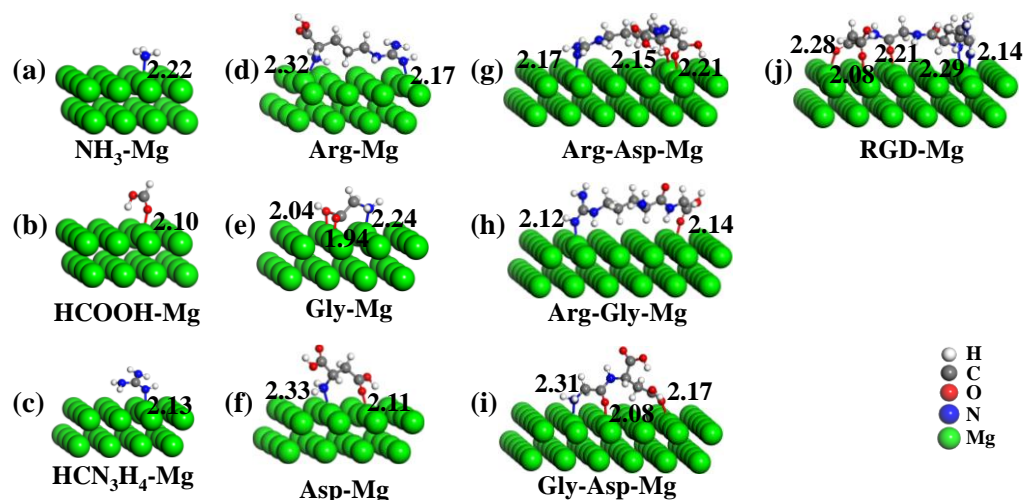


**Figure 2.** Stable adsorption configurations of (a–c) functional groups, (d–f) amino acids, (g–i) dipeptides, and (j) RGD tripeptide on Mg(0001) surface. The bond lengths (in Å) are also given.

As shown in Figure 2, the N atom in NH<sub>3</sub>, the carbonyl O atom in HCOOH, and the N atom with double bonds in HCN<sub>3</sub>H<sub>4</sub> bond to the Mg atoms of the surface. The amino acids, dipeptides, and RGD tripeptide mainly interacted with the Mg(0001) surfaces through functional groups. The theoretical radii for covalent bonding of N, O, and Mg atoms are 0.75 Å, 0.73 Å, and 1.36 Å, respectively. The theoretical bond lengths for covalent bonding of N-Mg and O-Mg atoms were 2.11 Å and 2.09 Å [46]. The calculated bond lengths of N-Mg and O-Mg were in the range 2.13–2.33 Å and 1.94–2.28 Å in the case of adsorption molecules on Mg(0001) surfaces. This result was very close to the theoretical bond length for the formation of covalent bonds of N-Mg and O-Mg, and the -NH<sub>2</sub> and -C=NH groups in HCN<sub>3</sub>H<sub>4</sub> play a crucial role in stabilizing the adsorption process.

The  $E_{ads}$  were calculated by using Equation (1), and the corresponding  $E_{ads}$  of functional groups, amino acids, dipeptides, and RGD tripeptide are shown in Tables 1–3, respectively. For the  $E_{ads}$  of functional groups in Table 1, the order of absolute values of  $E_{ads}$  was:  $E_{ads}(\text{HCN}_3\text{H}_4) > E_{ads}(\text{NH}_3) > E_{ads}(\text{HCOOH})$ . The  $E_{ads}$  of NH<sub>3</sub> on the Mg surface (−0.71 eV) was similar to the  $E_{ads}$  of NH<sub>3</sub> on the Cu surface (−0.78 eV) calculated by Nilsson et al. [47]. The  $E_{ads}$  of HCOOH on the Mg(0001) surface (−0.64 eV) was not significantly different from the  $E_{ads}$  of HCOOH on the Cu surface (−0.48 eV) calculated by Jiang et al. [48]. For the  $E_{ads}$  of amino acids in Table 2, the order of absolute values of  $E_{ads}$  was:  $E_{ads}(\text{Arg}) > E_{ads}(\text{Asp}) > E_{ads}(\text{Gly})$ . The  $E_{ads}$  of each amino acid was greater than that of the functional groups. For the dipeptides and RGD tripeptide, the amino acids cannot reach the optimal adsorption state simultaneously during the adsorption, resulting in the  $E_{ads}$  being greater than the sum of  $E_{ads}$  of the amino acid due to the constraint of chain length. A similar phenomenon also occurred in the adsorption of RGD tripeptide.

**Table 1.** The  $E_{ads}$  of functional groups on the Mg(0001) surface.

	Adsorption of Functional Groups		
	NH <sub>3</sub>	HCOOH	HCN <sub>3</sub> H <sub>4</sub>
$E_{ads}$ (eV)	−0.71	−0.64	−1.08

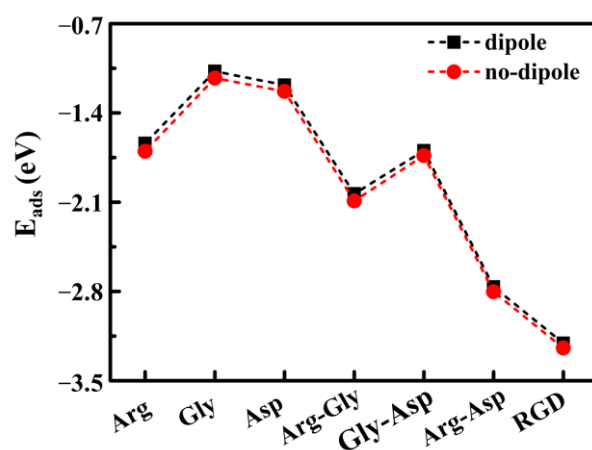
**Table 2.** The  $E_{ads}$  of amino acids on the Mg(0001) surface.

	Adsorption of Amino Acids		
	B	Gly	Asp
$E_{ads}$ (eV)	−1.67	−1.16	−1.23

**Table 3.** The  $E_{ads}$  of dipeptides and tripeptide on the Mg(0001) surface.

	Adsorption of Dipeptides and RGD Tripeptide			
	Arg-Asp	Arg-Gly	Gly-Asp	RGD
$E_{ads}$ (eV)	−2.80	−2.09	−1.73	−3.24

It is known that dipoles play a crucial role in the binding process due to the presence of dipoles and the chemical activity of groups. As the length of molecular chains and the complexity of spatial configurations increase, the probability of non-coincidence of positive and negative charge centers increases, which may affect the adsorption behavior of molecules on the surface. In order to analyze the influence of the above factors, dipole correction was added perpendicular to the surface to study the effect of this parameter on the  $E_{ads}$  of molecules on the Mg(0001) surface. The results were compared with those without dipole correction, as shown in Figure 3.

**Figure 3.** The  $E_{ads}$  of amino acids, dipeptides, and RGD tripeptide on the Mg(0001) surface with the dipole modification.

From the calculated results in Figure 3, it can be seen that the addition of dipole correction slightly increased the  $E_{ads}$  of amino acids, dipeptides, and RGD tripeptide on the Mg(0001) surface. However, the effect was very small and did not change the trend of  $E_{ads}$  changes. This result indicates that the adsorption process studied was mainly a chemical adsorption process. In view of this, there was no need to add dipole correction parameters in the subsequent calculation process of the present work.

### 3.2. Effect of Alloying Elements on the Adsorption of Molecules on Mg(0001) Surfaces

Zn, Y, and Nd elements played a crucial role in the mechanical properties and biocompatibility of Mg-based alloys, and their electronegativity in comparison with Mg was also representative [49]. In order to analyze the effect of the addition of Zn, Y, and Nd elements on the adsorption regularity of molecules on the Mg-based alloy surface, the selection of alloy content referred to the literature [50].

For the adsorption of functional groups on the Mg-based alloy surfaces, the optimized adsorption configurations are depicted in Figure 4 and the calculated corresponding  $E_{ads}$  are listed in Table 4. The bond lengths of functional groups on the Mg-based alloy surfaces

reported in Figure 4 were close to the theoretical bond lengths for covalent bonding of N-Mg, O-Mg, Y-Mg, and Nd-Mg atoms [46]. For the surface of Mg-Zn alloy, Zn with higher electronegativity obtained some electrons from the surrounding Mg atoms, causing a large number of electrons to accumulate around the Zn. It was easy for functional groups to be adsorbed on the Mg atoms which were around Zn atoms, and the addition of Zn enhanced the ability of functional groups to share electrons with surface Mg atoms to improve the  $E_{ads}$ . For the surfaces of Mg-Y and Mg-Nd alloys, it was easy for Y/Nd to transfer electrons to the surrounding Mg atoms due to the smaller electronegativity value. The ability to sharing electrons with the Mg-Y/Mg-Nd alloy surfaces was enhanced when functional groups directly interacted with Y/Nd atoms, making it easy to form the chemical bonds.

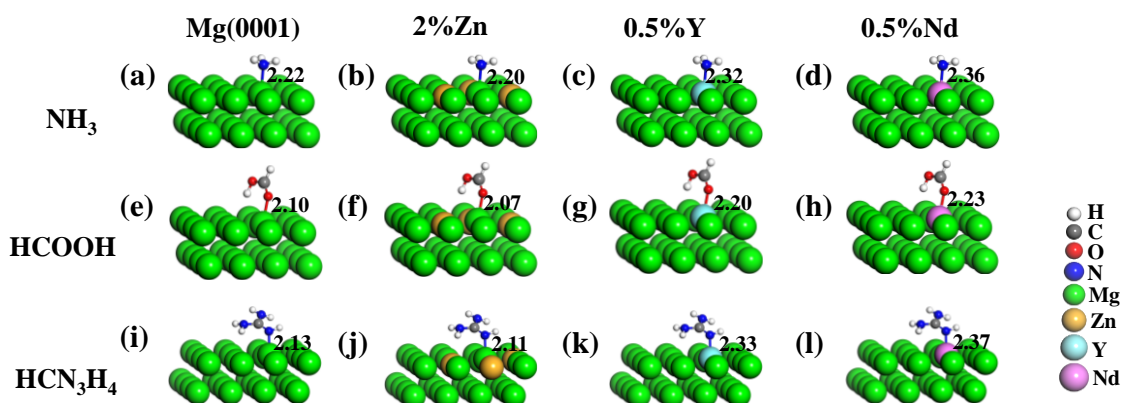


**Figure 4.** Stable adsorption configurations of functional groups of (a–d)  $\text{NH}_3$ , (e–h)  $\text{HCOOH}$ , and (i–l)  $\text{HCN}_3\text{H}_4$  on the Mg and Mg-based alloy surfaces containing 2% Zn, 0.5% Y, and 0.5% Nd. The bond lengths (in Å) are also given.

**Table 4.** The  $E_{ads}$  of functional groups on Mg and Mg-based alloy surfaces.

	$E_{ads}$ (eV)			
	Mg(0001)	2% Zn	0.5% Y	0.5% Nd
$\text{NH}_3$	−0.71	−0.83	−1.19	−1.22
$\text{HCOOH}$	−0.64	0.72	−1.21	−1.17
$\text{HCN}_3\text{H}_4$	−1.08	−1.19	−1.70	−1.76

The initial configurations of Arg, Gly, and Asp adsorbed on the surfaces of Mg-Zn, Mg-Y, and Mg-Nd alloys were consistent with that on the Mg(0001) surface. The optimized stable adsorption configurations are shown in Figure 5 and the calculated corresponding  $E_{ads}$  values are listed in Table 5. The surface of Mg and Mg-based alloy surfaces became rough, and the bound Mg atoms were shifted up by about 0.10 Å due to the adsorption of Arg, Gly, and Asp. The charge on the surface of Mg-Zn alloy was redistributed and the bond lengths between molecules and the surfaces of Mg-Zn alloy were reduced. The reduced bond lengths were in the range of 0.01–0.07 Å, which enhanced the interaction of adsorbed molecules and Mg-based alloy surfaces.

The  $E_{ads}$  of Arg, Gly, and Asp on the Mg-Zn, Mg-Y, and Mg-Nd alloy surfaces are listed in Table 5. Compared with that on the Mg(0001) surface, it was revealed that the interaction of configurations on the Mg-based alloy surfaces was enhanced and the promoting effect may become more effective by adding elements with smaller electronegativity. On the Mg-Zn alloy surface, Zn obtained some electrons from surrounding Mg atoms, which made it easier for N and O atoms in amino acids to share electrons with surface-bound Mg atoms due to the higher electronegativity of Zn (1.65) compared with Mg (1.31) [51]. Meanwhile, in the case of the Mg-Y and Mg-Nd alloy surfaces, the amino acids preferred to interact with the Y/Nd element directly instead of the surrounding Mg atoms.

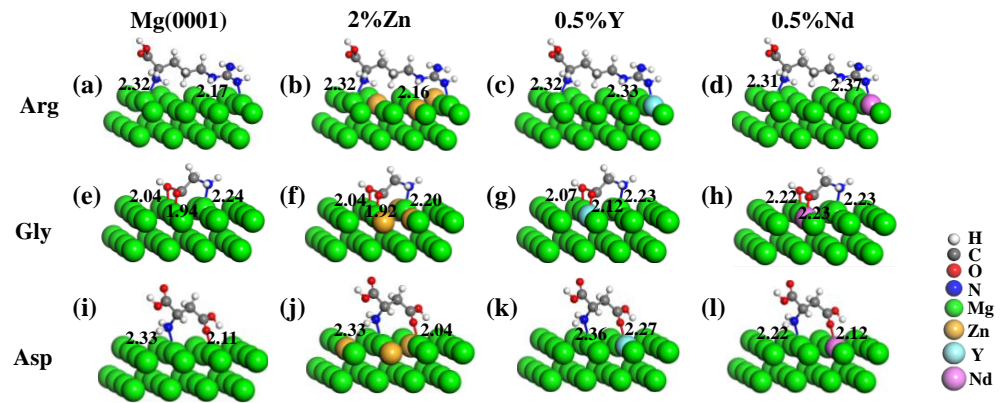


**Figure 5.** Stable adsorption configurations of amino acids of (a–d) Arg, (e–h) Gly, and (i–l) Asp on Mg and Mg-based alloy surfaces containing 2% Zn, 0.5% Y, and 0.5% Nd. The bond lengths (in Å) are also given.

**Table 5.** The  $E_{ads}$  of amino acids on Mg and Mg-based alloy surfaces.

	$E_{ads}$ (eV)			
	Mg (0001)	2% Zn	0.5% Y	0.5% Nd
Arg	−1.67	−1.99	−2.39	−2.37
Gly	−1.16	−1.35	−2.30	−1.77
Asp	−1.23	−1.39	−1.72	−2.02

For the adsorption of dipeptides and RGD tripeptide on the Mg-based alloy surfaces, the stable adsorption configurations are depicted in Figure 6. For the Mg–Y and Mg–Nd alloy surfaces, the distance ranges of N–Y, N–Nd, O–Y, and O–Nd were 2.32 Å~2.34 Å, 2.32 Å~2.38 Å, 2.12 Å~2.27 Å, and 2.12 Å~2.26 Å, respectively. These optimized bond lengths were very close to the theoretical covalent bond lengths for N–Y, N–Nd, O–Y, and O–Nd (2.37 Å, 2.39 Å, 2.35 Å, and 2.37 Å) [46]. From the calculated  $E_{ads}$  in Table 6, it was shown that the addition of Zn, Y, and Nd enhanced the interaction of dipeptides and RGD tripeptide on the Mg-based alloy surfaces. The  $E_{ads}$  of dipeptides and RGD tripeptide on the Mg-based alloy surface was significantly improved due to the redistribution of charges on the surface.

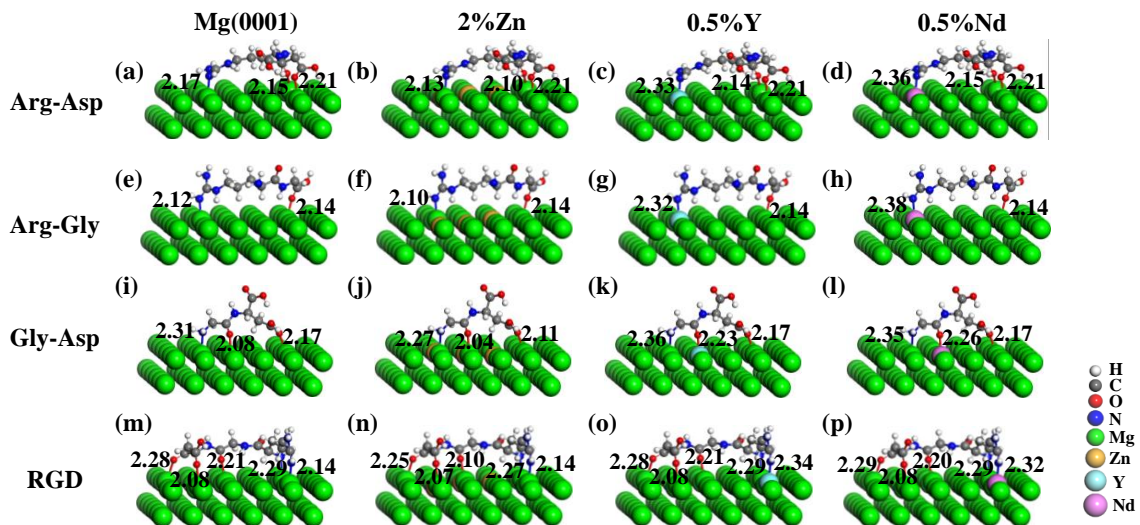


**Figure 6.** Stable adsorption configurations of dipeptides of (a~d) Arg-Asp, (e~h) Arg-Gly, and (i~l) Gly-Asp, and RGD tripeptide (m~p) on Mg and Mg-based alloy surfaces containing 2% Zn, 0.5% Y, and 0.5% Nd.

**Table 6.** The  $E_{ads}$  of dipeptides and RGD on Mg and Mg-based alloy surfaces.

	$E_{ads}$ (eV)			
	Mg(0001)	2% Zn	0.5% Y	0.5% Nd
Arg-Asp	−2.80	−3.06	−3.41	−3.53
Arg-Gly	−2.09	−2.29	−2.73	−2.85
Gly-Asp	−1.73	−2.13	−2.27	−2.45
RGD	−3.24	−3.73	−3.89	−4.03

Based on the calculated results, the addition of alloying elements affected the ability to share the lone pair electrons of N or O atoms in molecules with Mg atoms of the alloy surface. It can be concluded that molecules were easily adsorbed on the Mg atoms around the alloy elements when alloy elements with higher electronegativity than Mg (such as Zn) were added. However, the surface charges were redistributed by adding alloying elements with smaller electronegativity than Mg (such as Y and Nd), which affected the electronic structural properties of the Mg-based alloy surface. The electrons of the Mg-Y/Mg-Nd surfaces were more active. Meanwhile, molecules easily interacted directly with the alloy elements with smaller electronegativity on the Mg-based alloy surface.

### 3.3. Electronic Properties of Molecules on the Mg(0001) Surface

In order to study the electronic structural properties of molecules on Mg and Mg-based alloy surfaces, the projected density of states (PDOS) of  $\text{HCN}_3\text{H}_4$  and surface binding Mg atoms before and after adsorption were investigated as an example. The changes in the PDOS of the  $-\text{CN}=\text{NH}$  group in  $\text{HCN}_3\text{H}_4$  before and after adsorption on the Mg(0001) surface are shown in Figure 7.

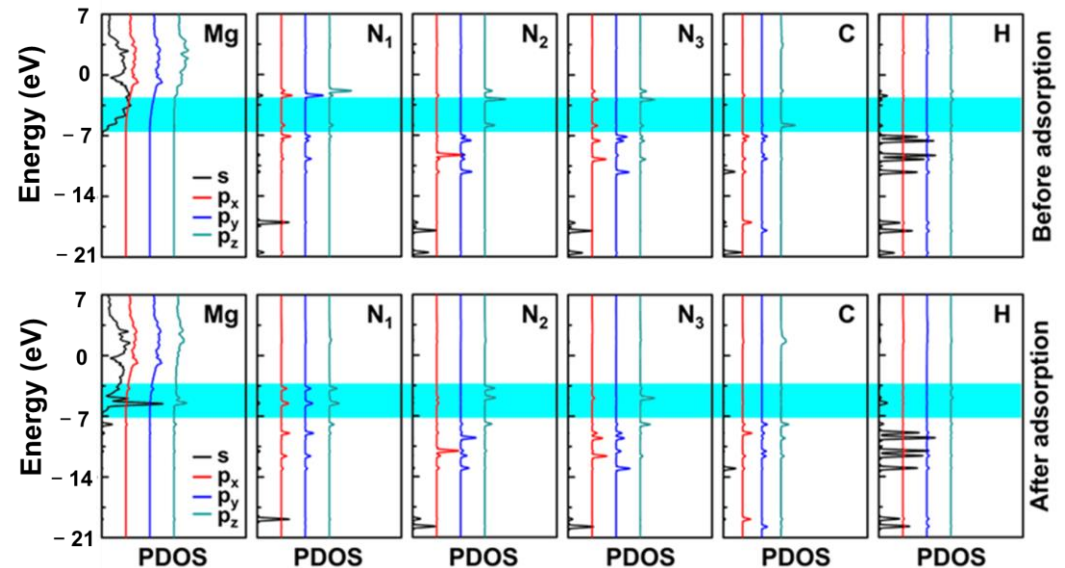


**Figure 7.** The PDOS of  $\text{HCN}_3\text{H}_4$  on the Mg(0001) surface before and after the adsorption. The Fermi level was set at 0 eV. The blue shaded area was the sharing of electrons and the formation of a chemical bond.

According to the calculated PDOS in Figure 7, both N atoms in the  $-\text{CN}=\text{NH}$  group contained lone pair electrons and this made it easy to share electrons with the Mg(0001) surface during the interaction. The Mg atom exhibited new peaks at the positions of  $-5.60$  eV and  $-5.90$  eV, while the  $\text{N}_1$  atom (labeled atom in Figure 1c) split into two peaks from the previous peak and moved towards lower energy positions. A new electronic state was formed at the position of  $-5.90$  eV. The  $\text{N}_3$  atom (labeled atom in Figure 1c) interacted with the Mg atom at  $-5.60$  eV, forming a new electronic state. The electronic

states moved downwards to lower energy positions when the entire system reached a stable state, resulting in a lower and more stable total energy of the system.

To further analyze the bonding mechanism and charge changes during the adsorption process between molecules and Mg surfaces, we calculated the charge density difference ( $\Delta\rho$ ) of the adsorption systems. The results are plotted in Figures 8–10. If  $\Delta\rho > 0$ , it indicates an increase in charge after the interaction; on the contrary, the charge decreased.  $\Delta\rho$  was obtained by using the following formula [45]:

$$\Delta\rho = \rho_{mol+sub} - \rho_{mol} - \rho_{sub} \quad (2)$$

where  $\rho_{mol+sub}$  is the charge density of the optimized adsorbate–substrate systems,  $\rho_{mol}$  is the charge density of the adsorbed molecule without the surface,  $\rho_{sub}$  is the charge density of the surface.

In Figure 8, the obvious light cyan area on the surface of the Mg atoms indicates the charge depletion of the binding Mg atoms; the yellow areas indicate the strong interaction of the functional groups and Mg(0001) surfaces. Similar phenomena were observed in the adsorption of amino acids, dipeptides, and RGD tripeptide on the Mg(0001) surfaces, as shown in Figures 9 and 10.

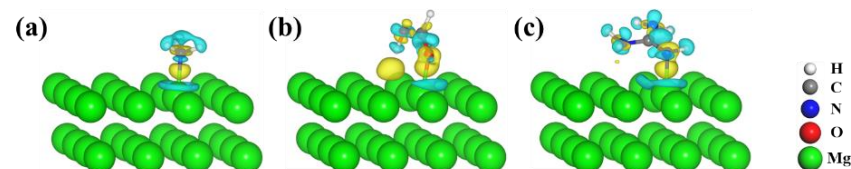


**Figure 8.** The charge difference of (a)  $\text{NH}_3$ , (b)  $\text{HCOOH}$ , and (c)  $\text{HCN}_3\text{H}_4$  adsorbed on the Mg(0001) surface. The value of the isosurface is  $\pm 0.003 \text{ e}/\text{\AA}^3$ , and the yellow and light cyan represent the accumulation and depletion of charge density.

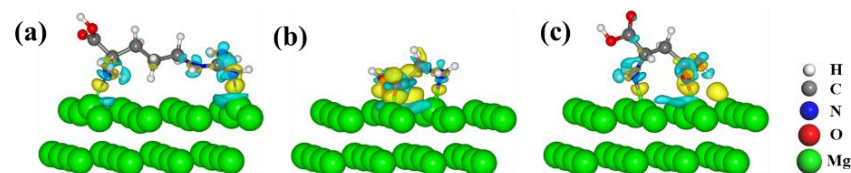


**Figure 9.** The charge difference of (a) Arg, (b) Gly, and (c) Asp adsorbed on the Mg(0001) surface. The value of the isosurface is  $\pm 0.03 \text{ e}/\text{\AA}^3$ , and the yellow and light cyan represent the accumulation and depletion of charge density.

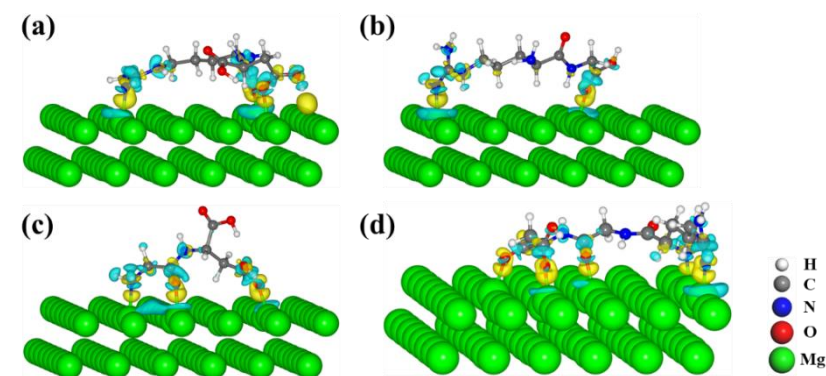


**Figure 10.** The charge difference of (a) Arg-Asp, (b) Arg-Gly, (c) Gly-Asp, and (d) RGD tripeptide adsorbed on the Mg(0001) surface. The value of the isosurface is  $\pm 0.003 \text{ e}/\text{\AA}^3$ , and the yellow and light cyan represent the accumulation and depletion of charge density.

#### 4. Conclusions

In this work, the influence of dipole correction and alloying elements on the interaction regularity of molecules on Mg and Mg alloys surfaces was assessed using the DFT approach. Conclusions based on the calculated results can be drawn as follows.

(1) The order of absolute values of computed  $E_{ads}$  of molecules varied in the following sequence:  $E_{ads}(\text{HCN}_3\text{H}_4) > E_{ads}(\text{NH}_3) > E_{ads}(\text{HCOOH})$ ;  $E_{ads}(\text{Arg}) > E_{ads}(\text{Asp}) > E_{ads}(\text{Gly})$ ;  $E_{ads}(\text{Arg-Asp}) > E_{ads}(\text{Arg-Gly}) > E_{ads}(\text{Gly-Asp})$ .

(2) Dipole correction slightly enhanced the interaction of molecules and Mg surfaces, but the trend of  $E_{ads}$  changes was not altered due to the constraint of chain length.

(3) The addition of alloying elements affected the charge distribution on the Mg surface and improved the interaction of molecules on Mg surfaces. Molecules easily directly interacted with the alloy elements with smaller electronegativity on Mg-based alloy surfaces.

**Author Contributions:** Conceptualization, E.L.; Software, Y.J.; Writing—original draft, Z.F.; Writing—review & editing, S.G.; Visualization, B.M.; Supervision, B.M. All authors have read and agreed to the published version of the manuscript.

**Funding:** This research was funded by the National Key Research and Development Program of China (2021YFC2400700), GHfund B (202302022245), Youth Fund Project of Zhongyuan University of Technology (K2022QN026) and Young Backbone Teacher Project of Zhongyuan University of Technology (2023XQG10). The calculations were supported by National Supercomputing Center in Zhengzhou.

**Institutional Review Board Statement:** Not applicable.

**Informed Consent Statement:** Not applicable.

**Data Availability Statement:** Data are contained within the article.

**Conflicts of Interest:** The authors declare no conflicts of interest.

#### References

1. Hao, D.K.; Lin, J.; Liu, R.W.; Pivetti, C.; Yamashiro, K.; Schutzman, L.M.; Sageshima, J.; Kwong, M.; Bahatyrevich, N.; Farmer, D.L.; et al. A bio-instructive parylene-based conformal coating suppresses thrombosis and intimal hyperplasia of implantable vascular devices. *Bioact. Mater.* **2023**, *28*, 467–479. [[CrossRef](#)] [[PubMed](#)]
2. Kim, S.Y.; Thangam, R.; Kang, N.Y.; Hong, H.; Kim, C.; Lee, S.K.Y.; Son, S.; Lee, H.J.; Tag, K.R.; Min, S.H.; et al. Modulation of macrophages by in situ ligand bridging. *Adv. Funct. Mater.* **2023**, *33*, 2215166. [[CrossRef](#)]
3. Sung, T.C.; Wang, T.; Liu, Q.; Ling, Q.D.; Subbiah, S.K.; Renuka, R.R.; Hsu, S.T.; Umezawa, A.; Higuchi, A. Cell-binding peptides on the material surface guide stem cell fate of adhesion, proliferation and differentiation. *J. Mater. Chem. B* **2023**, *11*, 1389–1415. [[CrossRef](#)] [[PubMed](#)]
4. Zhang, Z.Q.; Wang, H.Y.; Wang, L.; Chen, X.B.; Guan, S.K.; Lin, C.G.; Zeng, R.C. Protein conformation and electric attraction adsorption mechanisms on anodized magnesium alloy by molecular dynamics simulations. *J. Magnes. Alloys* **2022**, *10*, 3143–3155. [[CrossRef](#)]
5. Raikar, A.S.; Priya, S.; Bhilegaonkar, S.P.; Somnache, S.N.; Kalaskar, D.M. Surface Engineering of Bioactive Coatings for Improved Stent Hemocompatibility: A Comprehensive Review. *Materials* **2023**, *16*, 6940. [[CrossRef](#)]
6. Chen, J.; Liu, X.H.; Hong, Q.X.; Meng, L.J.; Ji, Y.; Wang, L.T.; Zhang, Q.Y.; Lin, J.F.; Pan, C.J. Synthesizing a multifunctional polymer to construct the catalytically NO-generating coating for improving corrosion resistance and biocompatibility of the magnesium alloy stent materials. *Prog. Org. Coat.* **2023**, *186*, 108058. [[CrossRef](#)]
7. Fang, H.; Wang, C.X.; Zhou, S.C.; Zheng, Z.; Lu, T.; Li, G.; Tian, Y.H.; Suga, T. Enhanced adhesion and anticorrosion of silk fibroin coated biodegradable Mg-Zn-Ca alloy via a two-step plasma activation. *Corros. Sci.* **2020**, *168*, 108466. [[CrossRef](#)]
8. Li, H.T.; Si, S.H.; Yang, K.; Mao, Z.A.; Sun, Y.H.; Cao, X.R.; Yu, H.T.; Zhang, J.W.; Ding, C.; Liang, H.X.; et al. Hexafluoroisopropanol based silk fibroin coatings on AZ31 biomaterials with enhanced adhesion, corrosion resistance and biocompatibility. *Prog. Org. Coat.* **2023**, *184*, 107881. [[CrossRef](#)]
9. Li, D.; Dai, D.N.; Xiong, G.G.; Lan, S.Q.; Zhang, C. Composite nanocoatings of biomedical magnesium alloy implants: Advantages, mechanisms, and design strategies. *Adv. Sci.* **2023**, *10*, 2300658. [[CrossRef](#)]
10. Shahed, C.A.; Ahmad, F.; Günster, E.; Foudzi, F.M.; Ali, S.; Malik, K.; Harun, W.S.W. Antibacterial mechanism with consequent cytotoxicity of different reinforcements in biodegradable magnesium and zinc alloys: A review. *J. Magnes. Alloys* **2023**, *11*, 3038–3058. [[CrossRef](#)]

11. Fan, Z.W.; Zou, Y.B.; Liu, C.L.; Xiang, S.C.; Zhang, Z.J. Hydrogen-Bonded organic frameworks: Functionalized construction strategy by nitrogen-containing functional group. *Chem.—A Eur. J.* **2022**, *28*, e202200422. [[CrossRef](#)] [[PubMed](#)]
12. Wang, Z.K.; Dong, Y.; Wang, Y.Y. Collagen-based biomaterials for tissue engineering. *ACS Biomater. Sci. Eng.* **2023**, *9*, 1132–1150. [[CrossRef](#)] [[PubMed](#)]
13. Acet, Ö.; Shcharbin, D.; Zhogla, V.; Kirsanov, P.; Halets-Bui, I.; Acet, B.; Gök, T.; Bryszewska, M.; Odabasi, M. Dipeptide nanostructures: Synthesis, interactions, advantages and biomedical applications. *Colloids Surf. B-Biointerfaces* **2023**, *222*, 113031. [[CrossRef](#)] [[PubMed](#)]
14. Li, L.C.; Xie, L.; Zheng, R.L.; Sun, R.Q. Self-assembly dipeptide hydrogel: The structures and properties. *Front. Chem.* **2021**, *9*, 739791. [[CrossRef](#)]
15. Shams, E.; Barzad, M.S.; Mohamadnia, S.; Tavakoli, O.; Mehrdadfar, A. A review on alginate-based bioinks, combination with other natural biomaterials and characteristics. *J. Biomater. Appl.* **2022**, *37*, 355–372. [[CrossRef](#)]
16. Yang, F.; Guo, G.Y.; Wang, Y.B. Inflammation-directed nanozyme-eluting hydrogel coating promotes vascular tissue repair by restoring reactive oxygen species homeostasis. *Chem. Eng. J.* **2023**, *454*, 140556. [[CrossRef](#)]
17. Chen, J.J.; Hu, G.S.; Li, T.J.; Chen, Y.H.; Gao, M.; Li, Q.T.; Hao, L.J.; Jia, Y.G.; Wang, L.; Wang, Y.J. Fusion peptide engineered “statically-versatile” titanium implant simultaneously enhancing anti-infection, vascularization and osseointegration. *Biomaterials* **2021**, *264*, 120446. [[CrossRef](#)]
18. Liang, X.Y.; Yang, L.; Lei, Y.; Zhang, S.M.; Chen, L.; Hu, C.; Wang, Y.B. Biomimetic-modified bioprosthetic heart valves with Cysteine-Alanine-Glycine peptide for anti-thrombotic, endothelialization and anti-calcification. *Int. J. Biol. Macromol.* **2023**, *250*, 126244. [[CrossRef](#)]
19. Yan, L.W.; Zhou, T.; Ni, R.C.; Jia, Z.R.; Jiang, Y.A.; Guo, T.L.; Wang, K.F.; Chen, X.; Han, L.; Lu, X. Adhesive Gelatin-Catechol complex reinforced poly(Acrylic Acid) hydrogel with enhanced toughness and cell affinity for cartilage regeneration. *ACS Appl. Bio Mater.* **2022**, *5*, 4366–4377. [[CrossRef](#)]
20. Aghaei, M.; Ramezanitaghartapeh, M.; Javan, M.; Hoseininezhad-Namin, M.S.; Mirzaei, H.; Rad, A.S.; Soltani, A.; Sedighi, S.; Lup, A.N.K.; Khori, V.; et al. Investigations of adsorption behavior and anti-inflammatory activity of glycine functionalized Al<sub>12</sub>N<sub>12</sub> and Al<sub>12</sub>ON<sub>11</sub> fullerene-like cages. *Spectrochim. Acta Part A Mol. Biomol. Spectrosc.* **2021**, *246*, 119023. [[CrossRef](#)]
21. Wang, Z.Q.; Song, T.; Guo, Z.W.; Cao, K.K.; Chen, C.; Feng, Y.G.; Wang, H.; Yin, F.K.; Zhou, S.; Dai, J.; et al. Targeting the allosteric pathway that interconnects the core- functional scaffold and the distal phosphorylation sites for specific dephosphorylation of Bcl-2. *J. Med. Chem.* **2020**, *63*, 13733–13744. [[CrossRef](#)] [[PubMed](#)]
22. Liu, B.; Jiang, M.; Zhu, D.Z.; Zhang, J.M.; Wei, G. Metal-organic frameworks functionalized with nucleic acids and amino acids for structure- and function-specific applications: A tutorial review. *Chem. Eng. J.* **2022**, *428*, 131118. [[CrossRef](#)]
23. Schweitzer-Stenner, R. The relevance of short peptides for an understanding of unfolded and intrinsically disordered proteins. *Phys. Chem. Chem. Phys.* **2023**, *25*, 11908–11933. [[CrossRef](#)] [[PubMed](#)]
24. Huang, L.L.; Yi, J.H.; Gao, Q.; Wang, X.D.; Chen, Y.S.; Liu, P. Carboxymethyl chitosan functionalization of CPED-treated magnesium alloy via polydopamine as intermediate layer. *Surf. Coat. Technol.* **2014**, *258*, 664–671. [[CrossRef](#)]
25. Guo, X.; Hu, Y.P.; Yuan, K.Z.; Qiao, Y. Review of the Effect of Surface Coating Modification on Magnesium Alloy Biocompatibility. *Materials* **2022**, *15*, 3291. [[CrossRef](#)] [[PubMed](#)]
26. Lin, Z.S.; Wang, T.L.; Yu, X.M.; Sun, X.T.; Yang, H.Z. Functionalization treatment of micro-arc oxidation coatings on magnesium alloys: A review. *J. Alloys Compd.* **2021**, *879*, 160453. [[CrossRef](#)]
27. Farwa, U.; Lee, H.Y.; Lim, H.; Park, I.; Park, S.; Moon, B.G.; Lee, B.T. Poly(L-lactide)/polycaprolactone based multifunctional coating to deliver paclitaxel/VEGF and control the degradation rate of magnesium alloy stent. *Int. J. Biol. Macromol.* **2023**, *250*, 126218. [[CrossRef](#)] [[PubMed](#)]
28. Yuan, J.; Dai, B.; Cui, X.F.; Li, P. The effects of electrodeposition temperature on morphology and corrosion resistance of calcium phosphorus coatings on magnesium alloy: Comparative experimental and molecular dynamics simulation studies. *RSC Adv.* **2021**, *13*, 34145–34156. [[CrossRef](#)]
29. Wang, Y.W.; Tang, Q.L.; Xu, X.C.; Weng, P.L.; Ying, T.; Yang, Y.; Zeng, X.Q.; Zhu, H. Accelerated discovery of magnesium intermetallic compounds with sluggish corrosion cathodic reactions through active learning and DFT calculations. *Acta Mater.* **2023**, *255*, 119063. [[CrossRef](#)]
30. Mamad, D.M.; Omer, R.A.; Othman, K.A. Quantum chemical analysis of amino acids as anti-corrosion agents. *Corros. Rev.* **2023**, *41*, 703–717. [[CrossRef](#)]
31. Méthivier, C.; Cornette, P.; Costa, D.; Landoulsi, J. Electrospray ion beam deposition of small peptides on solid surfaces: A molecular level description of the glutathione/copper interface. *Appl. Surf. Sci.* **2023**, *612*, 155895. [[CrossRef](#)]
32. Fang, Z.; Wang, J.F.; Yang, X.F.; Sun, Q.; Jia, Y.; Liu, H.R.; Xi, T.F.; Guan, S.K. Adsorption of arginine, glycine and aspartic acid on Mg and Mg-based alloy surfaces: A first-principles study. *Appl. Surf. Sci.* **2017**, *409*, 149–155. [[CrossRef](#)]
33. Fang, Z.; Wang, J.F.; Zhu, S.J.; Yang, X.F.; Jia, Y.; Sun, Q.; Guan, S.K. A DFT study of the adsorption of short peptides on Mg and Mg-based alloy surfaces. *Phys. Chem. Chem. Phys.* **2018**, *20*, 3602–3607. [[CrossRef](#)] [[PubMed](#)]
34. Fang, Z.; Zhao, Y.; Wang, H.Y.; Wang, J.F.; Zhu, S.J.; Jia, Y.; Cho, J.Y.; Guan, S.K. Influence of surface charge density on ligand-metal bonding: A DFT study of NH<sub>3</sub> and HCOOH on Mg (0001) surface. *Appl. Surf. Sci.* **2019**, *470*, 893–898. [[CrossRef](#)]
35. Fang, Z.; Wei, W.T.; Qiao, H.J.; Liang, E.R.; Jia, Y.; Guan, S.K. Effect of vacancy defects and hydroxyl on the adsorption of Glycine on Mg(0001): A first-principles study. *Coatings* **2023**, *13*, 1684. [[CrossRef](#)]

36. Kresse, G.; Hafner, J. Ab-initio molecular-dynamics simulation of the liquid-metal amorphous-semiconductor transition in germanium. *Phys. Rev. B* **1994**, *49*, 14251–14269. [[CrossRef](#)] [[PubMed](#)]
37. Kresse, G.; Furthmüller, J. Efficient iterative schemes for ab initio total-energy calculations using a plane-wave basis set. *Phys. Rev. B* **1996**, *54*, 11169–11186. [[CrossRef](#)] [[PubMed](#)]
38. Kresse, G.; Furthmüller, J. Efficiency of ab-initio total energy calculations for metals and semiconductors using a plane-wave basis set. *Comput. Mater. Sci.* **1996**, *6*, 15–50. [[CrossRef](#)]
39. Blochl, P.E. Projector augmented-wave method. *Phys. Rev. B* **1994**, *50*, 17953–17979. [[CrossRef](#)]
40. Perdew, J.P.; Burke, K.; Ernzerhof, M. Generalized gradient approximation made simple. *Phys. Rev. Lett.* **1997**, *78*, 1396. [[CrossRef](#)]
41. Lüder, J.; Sanyal, B.; Eriksson, O.; Puglia, C.; Brena, B. Comparison of van der Waals corrected and sparse-matter density functionals for the metal-free phthalocyanine/gold interface. *Phys. Rev. B* **2014**, *89*, 045416. [[CrossRef](#)]
42. Sowmiya, M.; Senthilkumar, K. Adsorption of RGD tripeptide on anatase (001) surface—A first principle study. *Comput. Mater. Sci.* **2015**, *104*, 124–129. [[CrossRef](#)]
43. Swanson, H.E.; McMurdie, H.F.; Morris, M.C.; Evans, E.H. Standard X-ray Diffraction Powder Patterns. In *National Bureau of Standards Monograph 25—Section 6*; U.S. Department of Commerce, National Bureau of Standards: Gaithersburg, MD, USA, 1968.
44. Madden, D.C.; Temprano, I.; Sacchi, M.; Jenkins, S.J. Spontaneous local symmetry breaking: A conformational study of Glycine on Cu{311}. *J. Phys. Chem. C* **2015**, *119*, 13041–13049. [[CrossRef](#)]
45. Höfiling, B.; Ortman, F.; Hannewald, K.; Bechstedt, F. Single cysteine adsorption on Au(110): A first-principles study. *Phys. Rev. B* **2010**, *81*, 045407. [[CrossRef](#)]
46. Sargent, W. *Table of Periodic Properties of the Elements*; Sargent-Welch Scientific: Skokie, IL, USA, 1980.
47. Nilsson, A.; Pettersson, L.G.M. Chemical bonding on surfaces probed by X-ray emission spectroscopy and density functional theory. *Surf. Sci. Rep.* **2004**, *55*, 49–167. [[CrossRef](#)]
48. Jiang, Z.; Qin, P.; Fang, T. Decomposition mechanism of formic acid on Cu (111) surface: A theoretical study. *Appl. Surf. Sci.* **2017**, *396*, 857–864. [[CrossRef](#)]
49. Zhao, N.; Zhu, D.H. Endothelial responses of magnesium and other alloying elements in magnesium-based stent materials. *Metallomics* **2015**, *7*, 113–123. [[CrossRef](#)]
50. Wang, B.; Guan, S.K.; Wang, J.; Wang, L.G.; Zhu, S.J. Effects of Nd on microstructures and properties of extruded Mg-2Zn-0.46Y-xNd alloys for stent application. *Mater. Sci. Eng. B-Adv. Funct. Solid-State Mater.* **2011**, *176*, 1673–1678. [[CrossRef](#)]
51. Allred, A.L. Electronegativity values from thermochemical data. *J. Inorg. Nucl. Chem.* **1961**, *17*, 215–221. [[CrossRef](#)]

**Disclaimer/Publisher’s Note:** The statements, opinions and data contained in all publications are solely those of the individual author(s) and contributor(s) and not of MDPI and/or the editor(s). MDPI and/or the editor(s) disclaim responsibility for any injury to people or property resulting from any ideas, methods, instructions or products referred to in the content.